Regular Article

PHYSICAL CHEMISTRY RESEARCH
Published by the
Iranian Chemical Society
www.physchemres.org
info@physchemres.org

Phys. Chem. Res., Vol. 13, No. 4, 721-729, December 2025
DOI: 10.22036/pcr.2025.530917.2698

Preparation and Characterization of CdS/SnO_2 Nanoparticles as Catalyst-degraded Products

F.M. Hussein[a], Y.K. Abdulamir[b], M.M. Radhi[c], R.R. ALAni[d] and E.A.J. Al-Mulla[e,f,*]

[a]*Department of Chemistry, College of Science, Mustansiriyha University, Baghdad, Iraq*
[b]*Al-Turath University, Baghdad. Iraq*
[c]*Health and Medical Techniques College-Baghdad, Iraq*
[d]*Alnukhba University College, Baghdad, Iraq*
[e]*College of Health and Medical Techniques, Al-Furat Al-Awsat Technical University, 54001 An-Najaf, Iraq*
[f]*College of Medical Technology, The Islamic University, Najaf, Iraq*
(Received 21 June 2025, Accepted 31 August 2025)

CdS/SnO_2 nanoparticles were synthesized *via* the sol-gel method using thioglycerol as a complexing agent. The effects of CdS/SnO_2 nanoparticle concentration, initial concentration of p-nitro toluene, pH, and temperature were determined. The nanoparticles were characterized by using UV-visible reduction spectroscopy, atomic force microscopy technique (AFM), and scanning electron microscopy (SEM). Doping of CdS nanoparticles with SnO_2 leads to alteration in electronics, and absorption has a band gap of 4.1 eV. The average diameter of particles and average roughness of CdS/SnO_2 are (93.83 and 5.99) nm. The particle size measured by spectral techniques was approximately 40 nm. The photo degradation of p-nitrotoluene was noticed, and the kinetic studies indicated a reaction to pseudo-first-order and a decrease in the reaction rate with rising initial concentration for p-nitrotoluene. The rate of photo degradation decreased when the concentration of CdS/SnO_2 nanoparticles exceeded 0.075 g l^{-1}.

Keywords: CdS/SnO_2 nanoparticle, Sol-gel method, Kinetic study, Photo degradation, Surface area, AFM

INTRODUCTION

Various techniques have been used in the manufacture of nanomaterials, especially chemical and physical methods. A physical method was used to convert the micro-rifampicin to nanoparticles, which resulted in the 85.74 nm dimension of RF NPs [1-5].

Nanoparticles are beneficial to society as an alternative to metals in diverse fields.

Nanoparticles used as drug carriers have high stability, high carrier capacity, the feasibility of incorporation of both hydrophilic and hydrophobic substances, and the feasibility of variable routes of administration. Given the potential to be modified depending on application, organic-inorganic hybrid materials are hi-tech because they can simultaneously exhibit the properties of both materials in an inorganic molecule [6]. Oxide nanoparticles synthesized using various methods are useful because these nanoparticles exhibit good electrical, optical, and magnetic properties that deviate from those of their bulk counterparts [7]. Various approaches, such as changing the tempering temperature, doping the semiconductor, and surface capping by various organic or inorganic layers [8] have been used to enhance the stability of nanoparticles. Nano-sized semiconductor material has many different optical and electromagnetic properties compared with normal materials. It can be used to produce photovoltaic cells with high efficiency, especially the materials with dye sensitization [9]. Heterogeneous photocatalysis is one of the most prevalent oxidation processes used for removing organic pollutants. In this technique, the metal oxide semiconductor absorbs light and creates activity, resulting in the integral oxidation of organic

*Corresponding author. E-mail: almullaemad@atu.edu.iq

components present in wastewater [10].

Cadmium sulfide is an important direct intermediate bandgap (2.42 eV) with excellent thermal and chemical stability and strong optical absorption, and is used in solar cells and exhibits interesting physical and chemical properties, such as wide band non-linear optical effects [11-14]. CdS has been recommended due to its potential technological applications in field-effect transistors, solar cells, photovoltaic and light-emitting diode photo-catalysis, photoluminescence, infrared photodetectors, ecological, prospectors, and biological sensors [15]. SnO_2 is a promising semiconductor for photocatalytic removal of organic pollutants due to its unique optical properties, chemical and thermal stability, non-toxicity, and low-cost metal precursors.

CdS nanoparticles with narrow band gap energy, tunable size, and excellent optical and electronic properties are involved in photocatalytic processes such as dye degradation and hydrogen production. CdS/SnO_2 heterostructure nanoparticle as a visible light active photo catalyst for the removal of methylene blue dye [16]. Also, CdS@SnO_2 exhibited remarkably enhanced photocatalytic activity for the selective oxidation of benzyl alcohol (BA) under visible light irradiation [17,18].

The efficient charge separation in the SnO_2/CdS heterostructure revealed its higher photocatalytic activity degradation of Congo red dye was found to be 97% under UV light irradiation [19].

CdS-doped SnO_2 yielded the maximum sensing response of 377 with faster response and recovery times of 8 s and 107 s, respectively, toward 10 ppm of NO_2 at room temperature [20].

In this work, we report a sol-gel technique to prepare textured CdS/SnO_2 nanoparticles at room temperature. The surface morphology of the combination was analyzed using scanning electron microscopy (SEM), and the band gap was determined using UV-visible.

EXPERIMENTAL

Materials and Methods

Chemicals and materials. Merck Chemical Reagent Co., Ltd. provided the majority of the reagents. Such as Cadmium chloride, Sodium supplied, thioglycerol, and ethanol absolute. Sol-gel was utilized to create the nanoparticles using distilled water. P-nitro toluene with 99.5% purity, which was provided by Sigma-Aldrich.

(A) Synthesis of CdS nanoparticles: an aqueous solution of cadmium chloride ($CdCl_2$) and thioglycerol (TG) at a molar ratio of 2:1 was gradually added to the aqueous solution, followed by the addition of 0.1 mol of Na_2S solution with stirring. For six hours, the mixture was moved around at a reflux of 70 °C. Centrifugation (3500 rpm) for 15 min was used to separate the solids from the solution, and washing for a certain time with acetone eliminated the unreacted solvent. The CdS nanoparticle was collected as a yellow powder after drying and aging for 72 h.

(B) CdS/ SnO_2 nanoparticles were prepared by adding SnO_2 to an aqueous solution of $CdCl_2$ (0.2 g) dissolved in absolute ethanol in 60 ml deionized water, thioglycerol (TG) 5 drops, TG was added dropwise into the aqueous solution, and 0.1 mol of Na_2S solution was injected dropwise into the above solution for 60 min under stirring. Finally, the mixture was refluxed with stirring for six hours. at70 °C. The solid was separated from the solution by centrifuge (3500 rpm) for 20 min and was washed with acetone to get rid of the product of drying for 5 h and aging for 72 h. A nanoparticle, a CdS/ SnO_2, was collected.

The photocatalytic activity of the CdS/SnO_2catalysts can be enhanced by controlling the CdS nanoparticle dispersion on the SnO_2 surface. When the molar ratio was 2:1, the CdS nanoparticles were not effectively scattered, and most of them aggregated on the SnO_2 surface.

Characterization

The structure and surface morphology of the as-prepared crystalline nanoparticles were characterized by SEM (Sigma). The UV-Vis absorption spectra of nanocrystals were captured using a double-beam spectrophotometer (100 Conc./Varian, USA) and two quartz cells with a 10-mm path length in the wavelength range of 200-800 nm. The energy band gap Eg (eV) and atomic force microscopy (AFM) using an AA300 scanning probe microscope (Angstrom Advanced Inc.) were used to measure the average particle size. Utilizing Instrument NOVA Station A with nitrogen gas, the surface area of nanoparticles was examined. A 150 W medium-pressure mercury lamp supply from PHYWE (England) produced the UV light.

RESULTS AND DISCUSSION

Figure 1a shows the SEM images with the particle size distribution of CdS as plate nanocomposites. In Fig. 1b, CdS particles with irregular SnO_2 morphology were due to the agglomeration of primary particles, and the average diameter of 40 nm of CdS. CdS cores were coated with SnO_2 particles, and the average particle size of the colloidal nanoparticles was 67.6 nm. The CdS nanocrystals grown at 70 °C show the surface morphology of the nanoparticles. The discrepancy associated with the nano-sized CdS sample can be attributed to the non-spherical geometry of nanoparticles and epigraphical observation. However, Barman *et al.* reported that CdS with polyvinyl alcohol at 70 °C exhibited a spherical shape [21].

CdS/SnO_2 nanoparticles tend to agglomerate due to attractive forces between the particles, particularly van der Waals forces. This tendency is exacerbated during synthesis and processing, especially the sol-gel method and calcination, which can lead to clustering and poor dispersion. Nanoparticles can form in solution and then cluster together before they are fully dried and sintered. Non-spherical particles can experience stronger attractive forces and thus are more prone to agglomeration.

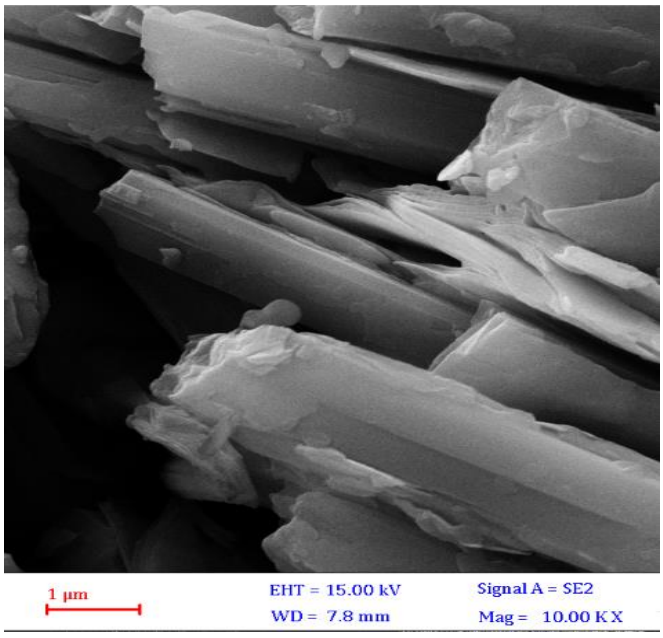

Fig. 1a. SEM image of CdS nanoparticle.

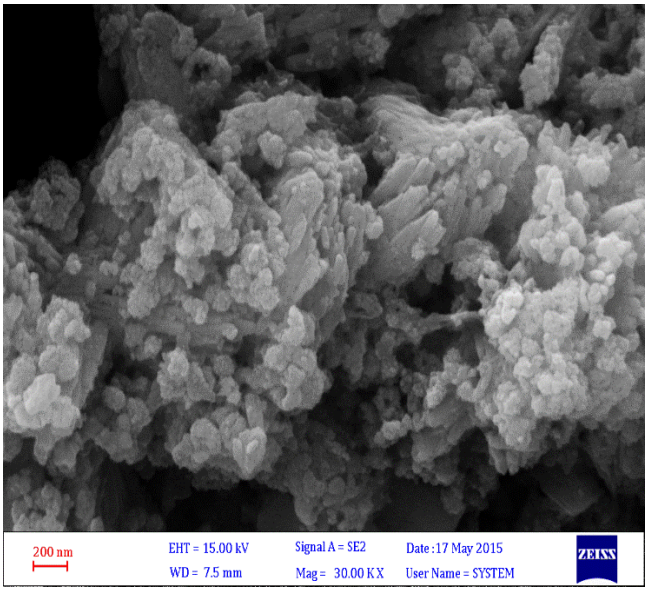

Fig. 1b. SEM image of CdS/SnO_2 nanoparticle.

The energy gap values of CdS and CdS/SnO_2 were measured using the absorption spectra of the nanoparticles. The band gap of the synthesized nanoparticles is calculated using the Taucs relation, [22] which is described in Eq. (1).

$$(\alpha h\nu)^{1/n} = A(h\nu - E_g) \quad (1)$$

Where A is a constant, E_g is the materials' band gap, and α is the absorption coefficient. The type of transition determines the exponent (n). CdS/SnO_2 nanoparticles have a band gap of 4.1 eV. This value changed in comparison to the energy gap of CdS (2.42 eV) and SnO_2 (3.52 eV). The sample's band gap shifted as a result of the particle size reduction.

Wavelength shifts across high-energy CdS nanoparticles initially favor spherical clusters, according to Efra [23]. With the effective masses of the valence band hole and the conduction band electron, this author assumed energy to both the valence and conduction bands. The coupled CdS/SnO_2 displayed catalytic action compared with the pure CdS or SnO_2 because the band gap of SnO_2 was 3.8 eV. Due to its minimum task function, CdS had a higher Fermi energy level than SnO_2, which caused electrons to move from the CdS conduction band to the SnO_2 conduction band, and hole transmission from the SnO_2 valence band to the CdS valence band took place [24].

The band gap of CdS nanoparticles can be tuned by controlling their size. Smaller nanoparticles exhibit a larger band gap compared to bulk CdS. For example, bulk CdS has a band gap of 2.42 eV, while nanoparticles can range from 3.12 eV (for 2.3 nm particles) down to 2.47 eV (for 6.0 nm particles). Some studies have reported a band gap of almost 3.9 eV for 1 nm cubic CdS nanoparticles. By carefully controlling the size of CdS nanoparticles, researchers can tailor their optical and electronic properties for specific applications.

Energy band gaps ranging between 3.12 eV and 2.47 eV have been obtained for the samples containing the nanoparticles in the range of 2.3 to 6.0 nm in size. A correlation between the band gap and size of the nanoparticles is also established [25].

The band gap of SnO_2 nanoparticles generally increases as particle size decreases due to quantum confinement effects. Bulk SnO_2 has a band gap of around 3.6 eV. Smaller nanoparticles exhibit higher band gaps, with values ranging from 3.7 eV to 4.2 eV or higher observed in some studies.

The band gap of SnO_2 nanoparticles is 4.51 eV. The band gap of SnO_2 nanoparticles is larger than that of their bulk equivalent due to the quantum confinement effects [26].

While Fig. 2 (A and B) atomic force microscope (AFM) based on using nanostructured probes to perform atomic-level surface scanning of materials [27]. With its great detail, AFM imaging seems especially appealing for characterizing particulate matter based on nanomaterials. These technologies would be useful, especially in determining the probe's contact forces with wide surface domains down to individual molecules, enabling timely assessment of interface characteristics. The average diameter of particles and average roughness of CdS are (75.28 and 0.69) nm, while CdS/SnO_2 (93.83 and 5.99) nm, which can be understood by considering that doping SnO_2 may diffuse into the grain boundaries of SnO, thereby growing the grains. This rough surface can be indicated in three-dimensional (3D) images of nanoparticle material that had an irregularly distributed CdS nanoparticle over the entire surface (Figs. 3A and B). This structural optimization may play an important role in more applications.

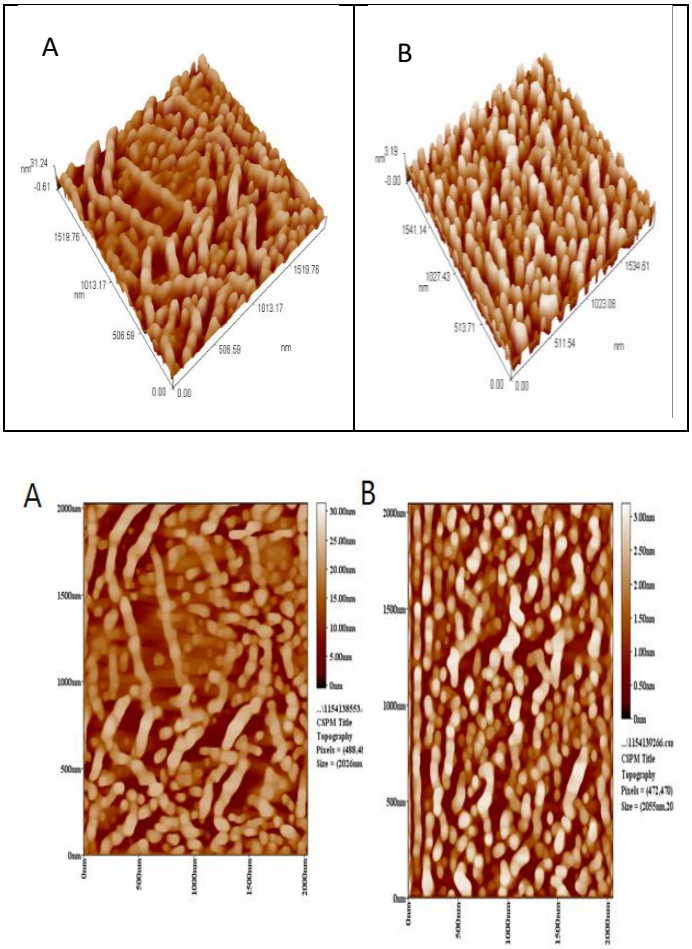

Fig. 2. AFM a verge particle size (A) CdS/SnO_2, (B) CdS nanoparticles.

(Barrett-Joyner-Halenda (BJH) Surface Analysis)

Figure 3 (A and B) shows the isotherm types of CdS and CdS/SnO_2 nanoparticles. The BJH specific surface area of CdS was 13.50 m^2 g^{-1} with a total pore volume of 0.0184 cm^3 g^{-1}, compared with 20.84 m^2 g^{-1} and 0.07323 cm^3 g^{-1}, respectively, for coupled CdS/SnO_2.

The aggregation of Sn particles increased the pore volume and formed a new surface morphology. The adsorption hysteresis curve type showed that the photo catalysts had uniformly sized, cylindrical pores. BET analysis quantifies the surface area of materials, crucial for understanding adsorption efficiency. A higher surface area generally leads to increased adsorption capacity and provides

more sites for adsorbate molecules to bind, where the presence of pores and surface area directly impacts the amount of pollutants they can remove. For CdS and CdS/SnO_2, the average pore widths were 8.711 nm and 28.48 nm, respectively. The condensation technique was used to create the mesoporous materials that were used as photo-catalysts. The surface area of CdS/SnO_2 was different from SnO_2, indicating that a portion of the CdS nanoparticle may have deposited inside the pores of SnO_2. Table 1 shows the physicochemical properties of CdS nanoparticles and CdS/SnO_2 prepared by the sol-gel method.

The coupled structure that has received the most attention is that consisting of CdS and SnO_2 colloidal particles. As illustrated in Scheme 1, it is possible to irradiate CdS with light of lower energy than that needed to electronically excite SnO_2 particles, so the photo-generated electron can be injected from CdS to SnO_2 while the hole remains in CdS. The electron transfer from CdS to SnO_2 increases the charge separation.

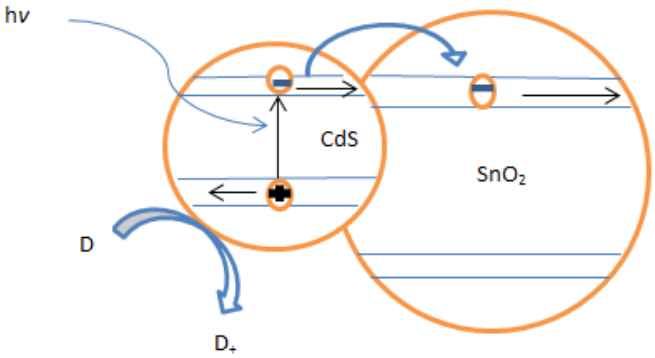

Scheme 1. Schematic illustration of the photo charge injection process that occurs upon excitation of the CdS component of a CdS/SnO_2

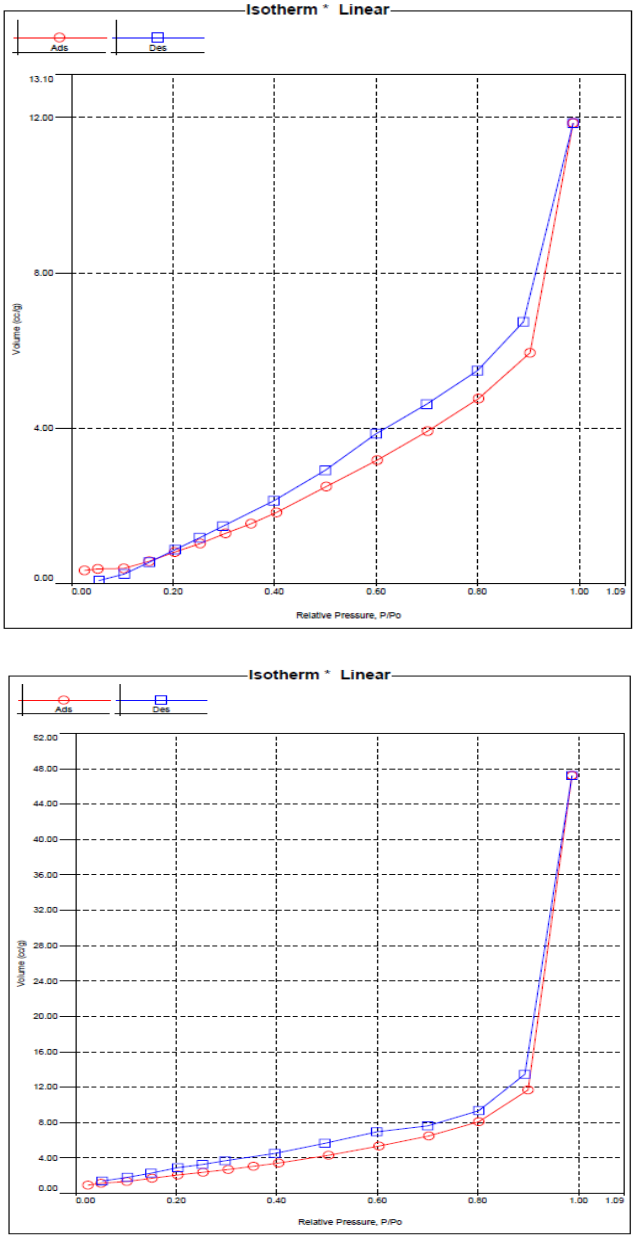

Fig. 3. A: The BJH curve and adsorption-desorption isotherm of CdS, B: adsorption-desorption isotherm and BJH curve of CdS/SnO_2.

Table 1. The Properties of CdS Nanoparticle and CdS/SnO_2 Prepared by Sol-gel

Compound	Surface area ($m^2 g^{-1}$)	Pore volume ($cm^3 g^{-1}$)	A verge pore width (nm)
CdS	13.50	0.0184	8.711
CdS/SnO_2	20.84	0.07323	28.48

Kinetic Study of p-Nitro toluene Degradation Using CdS/SnO_2

The photocatalytic reaction of p-nitrotoluene in aqueous solution follows the Langmuir-Hinshelwood model. The equation can be simplified to a first-order kinetic with an apparent rate constant.

$$\ln C_o/C_t = k_{app}\, t \qquad (2)$$

Where k_{app} is the apparent rate constant. The pseudo-first-order kinetics of p-nitrotoluene degradation were obtained. The apparent rate constants are reported in Table 2.

Table 2. Kinetic Constant of p-nitro Toluene Degradation by CdS/SnO_2 Nanoparticle

Concentration (mol./l) p-nitrotoluene	k_{app} (min^{-1}) × 10^{-3}
0.0001	6.3
0.0003	9.7
0.0005	6.8
0.0007	8.1

Effect of CdS/SnO_2 Nanoparticle Loading

The optimum loading of CdS/SnO_2 nanoparticles yields the highest photo degradation rate at the initial concentration of p-nitrotoluene of 0.075 g l^{-1}. Above this value, the rate of photodegradation gradually decreases.

The CdS/SnO_2 suspension became increasingly opaque to incident light; therefore, the light absorption was limited only to the first layers of the photocatalytic mixture, and the solution layers did not receive light photons (Fig. 4).

Effect of pH

The effect of pH on the photo-degradation reaction was also investigated. Results showed that the photolysis reaction did not change at pH values ranging from 3 to 9 at CdS/SnO_2 loading of 0.075 mg l^{-1} and an initial concentration of p-nitrotoluene at 3 × 10^{-4} M. Despite this finding, the initial rate of photo degradation steadily decreased as the pH value increased [28]. The pH reached its highest value of 5.2. These results are also presented in Fig. 5 and Table 3.

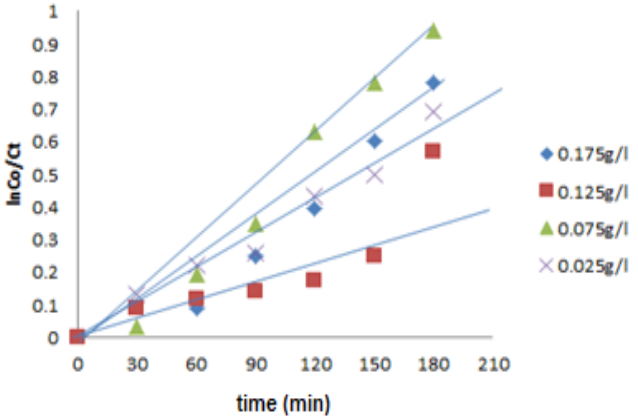

Fig. 4. The effect of loading of various nanoparticles CdS/SnO_2, p-nitro toluene 1 × 10^{-4}.

CdS/SnO_2 nanoparticles can have different surface charges depending on the pH. At higher pH (more alkaline conditions), the nanoparticles may become more negatively charged, which can affect their ability to interact with and adsorb certain pollutants, especially those that are also negatively charged. The degradation by photo catalysts CdS/SnO_2 often involves the generation of reactive-like hydroxyl radicals that degrade the pollutants. The efficiency of this process can be influenced by the pH, as it affects the surface properties of the catalyst.

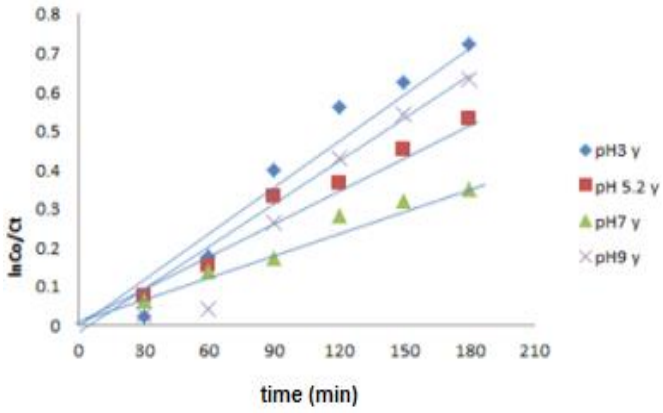

Fig. 5. The effect of pH for nanoparticle CdS/SnO_2,4-nitrotolune 3 × 10^{-4}.

Table 3. Different pH at Concentration of 4-Nitrotolune (3×10^4 M), CdS/SnO_2 Nanoparticle (0.075 g l^{-1})

pH	Rate (M min^{-1}) × 10^{-7}	Efficiency%
3	14.4	51.4
5.2	29.1	78.4
7	6.0	29.38
9	13.5	46.63

Effect of Initial Concentration of p-Nitro Toluene

Table 4 shows that the concentration of p-nitro toluene increased, and also the initial rate of photo-catalyst degradation increased with concentration.

The rate of a reaction involving p-nitro toluene generally increases with increasing concentration of p-nitro toluene because a higher concentration means more reactant molecules are available to participate in collisions that lead to product formation. In a chemical reaction, molecules must collide with sufficient energy and proper orientation for a reaction to occur. With a higher concentration of p-nitro toluene, there are simply more molecules present in a given volume, leading to more frequent collisions between p-nitro toluene molecules and the catalyst.

Table 4. The Various Concentrations of p-Nitrotoluene, CdS/SnO_2 Nanoparticle (0.075 g l^{-1})

Conc. of p-NT (M) × 10^{-4}	Rate (M min^{-1}) × 10^{-7}	Efficiency%
1	6.30	60.05
3	29.1	78.40
5	34.0	61.73
7	56.7	73.53

Effect of Temperature

The effect of temperature on the thermal degradation rate of p-nitrotoluene in the present CdS/SnO_2 nanoparticle is shown in Fig. 6. The experiments were carried out at different temperatures, about 288 K to 318 K. Table 5 shows the effect of temperature on the rate of decomposition of p-nitrotoluene at CdS/SnO_2 load (0.075 g l^{-1}) and a p-nitrotoluene concentration of 3×10^{-4} M. Activation energy equal to 33.308 kJ mol^{-1} obtained from the reaction rate constant vs. reciprocal temperature in an Arrhenius plot. That low value indicated that the heterogeneous process is generally independent of the temperature.

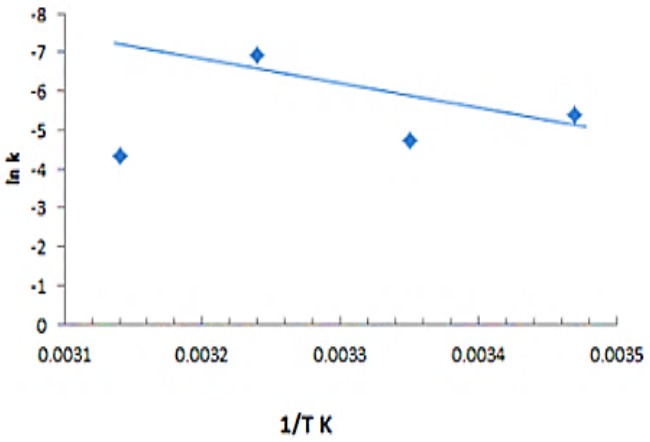

Fig. 6. Reaction rate constant against 1/T in an Arrhenius plot.

Table 5. The Effect of Temperature on Decomposition of p-Nitrotoluene, CdS/SnO_2 Nanoparticle (0.075 g l^{-1}), pH 5.2

Temperature (°K)	Rate (M min^{-1}) × 10^{-7}	Efficiency%
288	4.20	21.90
298	29.1	78.40
308	3.00	15.13
318	39.6	87.30

Photodegradation of p-Nitro Toluene under Solar Exposure

The photo degradation of p-nitrotoluene (3×10^{-4} M) under sunlight radiation was carried out in the presence of CdS/SnO_2 (0.075 g l^{-1}). Efficiency after 180 min was 76.6 W, whereas similar experimental conditions yielded efficiency values of 150 and 300 W. This activity was due to the absorption of solar energy by the combined CdS/SnO_2. The CdS nanoparticle exhibited low efficiency compared with the CdS/SnO_2 nanoparticle, and the results are shown in Table 6.

Table 6. efficiency and Rate of Light Sources for CdS/SnO_2 and CdS

Source (watt)	Rate (M min^{-1}) × 10^{-7}	Efficiency%
150	29.1	78.4
300	14.7	50.0
Sunlight	26.7	76.6
CdS (0.075 g l^{-1}), 150 watt	3.9	42.5

CONCLUSIONS

A modification of CdS nanoparticles and CdS/SnO_2 was conducted. The addition of SnO_2 as an electron donor can augment photocatalytic activity by reacting with charge recombination's valence band gap irreversibly. Doping CdS can increase photo reactivity in the visible spectrum and retain charge recombination. CdS and CdS/SnO_2 were synthesized by the sol-gel method at 70 °C. The prepared materials were characterized as hexagonal with particle sizes of 19.3 nm for CdS and 22.94 nm for CdS/SnO_2, leading to an increased band gap. However, the wavelength exhibited a blue shift to a decreased wavelength, which can be compared with the band gap of the distinct absorption of uncapped CdS. The surface area and total pore volume of CdS were 13.50 m^2 g^{-1} and 0.0184 cm^3 g^{-1}, whereas those of coupling CdS/SnO_2 were 20.84 m^2 g^{-1} and 0.07323 cm^3 g^{-1}, respectively. The study on p-nitrotoluene photo degradation provides a highly efficient method of degradation of toxic compounds. At pH 5.2 and 150 W, 0.075 g l^{-1} of CdS/SnO_2 nanoparticles decomposed p-nitrotoluene in 180 minutes, and the photo-catalyst-degraded products exhibited decreased toxicity.

ACKNOWLEDGEMENTS

The authors appreciate the staff of Mustansiriyah University's Department of Chemistry, College of Science, Iraq, for supporting this research.

REFERENCES

[1] Yousif, K. A.; Muhammed, M. R.; Emad, A. J., Use of Nano-Sensors of the Interferences between Pb(II) with Each of Mg(II), Zn(II), Mn(II), Ca(II), Co(II) and PO_4^{3-} in Blood Medium: An Electrochemical Study. *Nano Biomed.* **2017**, *9*(3), 199-207, DOI: 10.5101/nbe.v9i3.p199-207.

[2] Radhi, M. M.; Tan, W. T.; Rahman, M. Z. B.; Kassim, A. B., Electrochemical characterization of the redox couple of $[Fe(CN)_6]^{3-}/[Fe(CN)_6]^{4-}$ mediated by a grafted polymer modified glassy carbon electrode. *J. Chem.* **2010**, *43*(11), 927-931, DOI: 10.1252/jcej.10we150.

[3] Sali, N. J.; Muhammed, M. R.; Emad, A. J.; Ebaa, A. A., Rifampicin Nanoparticles: Thermodynamic Properties in KCl Electrolyte Using Cyclic Voltammetry. *Nano Biomed.* **2024**, *16*(1), 129-134, DOI: 10.26599/NBE.2024.9290046.

[4] Mohammed, A. H. Y.; Muhammed, M. R.; Emad, A. J. A., The Effect of Aluminum Nanoparticles on Vaccine-dosed Rabbits Investigated Using Cyclic Voltammetry. *Nano Biomed.* **2023**, *15*(1), 21-27, DOI: 10.26599/NBE.2023.9290004.

[5] Muhammed, M. R.; Anfal, I. I.; Majid, S. J.; Emad A. J. A.; Wisam H. H., Nano Cinnamon: A Study in Human Blood Medium Using Cyclic Voltammetry on Glassy Carbon Electrode (GCE). *Nano Biomed.* **2022**, *14*(2), 167-172, DOI:10.5101/nbe.v14i2.p167-172.

[6] Lee, S. H.; Jun, B. H., Silver nanoparticles: synthesis and application for nanomedicine. *Int. J. Mol. Sci.* **2019**, *20*(4), 865, DOI: 10.3390/ijms20040865.

[7] Qasmi, N. A.; Somro, M. T.; Ismail, I. M. I.; Danish, E. Y. A. A., An enhanced electro catalytic oxidation and determination of 2,4-dichlorophenol on multilayer deposited functionalized multi-walled carbon nanotube/Nafion composite film electrode. *Arab. J. Chem.* **2019**, *12*(7), 946-956, DOI: 10.1016/j.arabjc.2015.08.032.

[8] Fabrizio, R.; Filippo, G.; Giuseppe, G., Ion Implantation Doping in Silicon Carbide and Gallium Nitride Electronic Devices. *Micro.* **2022**, *2*(1), 23-53, Doi.org/10.3390/micro2010002.

[9] Chenlei, Z., Properties, Preparations and Applications of Nano-sized Semiconductor Material. *Int. Conf. Mater. Eng. Inf. Technol. Appl*., **2015**, 929-932, DOI: 10.2991/meita-15.2015.175.

[10] Nainani, R.; Thakur, P.; Chaskar, M., Synthesis of silver doped TiO_2 nanoparticles for the improved photocatalytic degradation of methyl orange. *J. Mater.*

Sci. Eng. B. **2012**, *2*(1), 52-58, doi.org/10.1080/19443994.2013.794115.

[11] Kahlaa, H. A.; Natheer, J. I.; Selma, M. H. J., Structural, Optical and Morphological Properties Cadmium Sulfide Thin Films Prepared by Hydrothermal Method. *J. Appl. Sci. Nanotechnology.* **2021**, *1*(2), 49-57, DOI: 10.53293/jasn.2021.3478.1021.

[12] Geremew, T.; Abza, T., Microstructural and Optical Characterization of Heterostructures of ZnS/CdS and CdS/ ZnS Synthesized by Chemical Bath DepositionMethod. *Adv. Mater. Sci. Eng.* 20, 11, DOI.org/10.1155/2020/1401689

[13] Murugesan, R.; Sivakumar, S.; Karthik, K.; Anandan, P.; Haris, M., Structural, Optical and Magnetic Behaviors of Fe/Mn-doped and Co-doped CdS Thin Films Prepared by Spray Pyrolysis Method. *Appl. Phys.* **2019**, *A 125*, 281, DOI:10.1007/s00339-019-2577-x.

[14] Ahmadi, L. K.; Hesar, R. M. Z.; Khademinia, S., Influence of Reaction Parameters on Crystal Phase Growth and Optical Properties of Ultrasonic- assisted Hydro- and Solv thermal Synthesized Sub micrometer-sized CdS Spheres. *Int. J. Nano Dimens.* **2018**, *9*(4), 346-356.

[15] Alejandro, C. V.; Raquel, E. G., Present and Perspectives of Photoactive Porous Composites Based on Semiconductor Nanocrystals and Metal-Organic Frameworks. *Molecules*. **2021**, *26*(18), 5620, DOI.org/10.3390/molecules26185620.

[16] Emad, E. El-Katori; Ahmed, M. A.; El-Bindary, A. A.; Aly, M. Oraby., Impact of CdS/SnO_2 Heterostructured Nanoparticle as Visible Light Active Photocatalyst for the Removal of Methylene Blue Dye. *Chemistry*. **2020**, *392*, 112403, DOI: 10.1016/j.jphotochem.2020.112403.

[17] Ya, L.; Ping, Z.; Baozhu, T.; Jinlong, Z., The Core-Shell Structural CdS@SnO_2 Exhibited Remarkably Enhanced Photocatalytic Activity for Selective Oxidation of Benzyl Alcohol to Benzaldehyde. *ACS Appl. Mater. Interfaces*. **2015**, *7*(25), DOI: 10.1021/acsami.5b04128.

[18] Xiaoming, Z.; Yannan, M.; Songbo, Z.; Lili, G.; Hong, C.; Jiajia, M.; Xin, Z.; Miao, Z.; Wenyan, L., CdS Nanoparticles Sensitized High Energy Facets Exposed SnO_2 Elongated Octahedral Nanoparticles Film for Photocatalytic Application. *Mater. Res. Bull.* **2019**, *111*, 118-125.

[19] Arik, K.; Simanta, K.; Amitava, P., Photocatalytic Properties of Semiconductor SnO_2/CdS Heterostructure Nanocrystals. *RSC Adv.* **2012**, *2*, 10222-10230.

[20] Ajay, K. S.; Jatinder, P.S.; Babita, S.; Sandeep, M.; Anjali, S., CdS-SnO_2Nanocomposite Sensor for Room Temperature Detection of NO_2 Gas. *Sensing Technol.* **2022**, 283-289, DOI:10.1007/978-3-030-98886-9_22

[21] Araa, H. H.; Majeed, A. H., Effect of CdS Nanoparticles on the Optical Properties of (PVA–PVP) Blends. *J. Mech. Eng. Res. Dev.* **2021**, *44*(3), 265-274.

[22] Makula, P.; Pacia, M.; Macyk, W., How to Correctly Determine the Band Gap Energy of Modified Semiconductor Photocatalysts Based on UV-Vis Spectra. *Phys. Chem. Lett.* **2018**, *9*(23), 6814-6817.

[23] Fengling, L.; Chao, H.; Panbo, S.; Guangxin, W.; Jiwen, L.; Qinghua, C., Spherical CdS Nanoparticles Precipitated from a Cadmium Thiosulfate Complex Using Ultraviolet Light for Photocatalytic Dye Degradation. *Metals*. **2023**, *13*(3), 554. DOI.org/10.3390/met13030554.

[24] Wang, C.; Shao, C.; Zhang, X., SnO_2Nanostructures-TiO_2 Nanofibers Heterostructures: Controlled Fabrication and High Photocatalytic Properties. *Inorg. Chem.* **2009**, *48*, 7261-7268, DOI: 10.1021/ic9005983.

[25] Dinesh, P.; Kuldeep, Rathore, S.; Saxena, N. S., Energy Band Gap Studies of CdS Nanomaterials. *J. Nano Res.* **2008**, *3*, 97-102.

[26] Priscy, L.; Osvaldo, N.; Soto, R. C. A.; Andres C. B., SnO_2 Nanoparticles Synthesized with Citrus aurantifolia and Their Performance in Photocatalysis. *J. Mater. Sci.: Mater. Electron.* **2020**, *27*(4), DOI: 10.1007/s10854-020-04242-5.

[27] Marica, M.; Vineenzo, G.; Luigi, A., Atomic Force Microscopy: A Powerful Tool to Address Scaffold Design in Tissue Engineering. *J. Funct. Biomater.* **2017**, *8*(7), 1-20, DOI.org/10.3390/jfb8010007.

[28]Khorsandi, H.; Teymori, M.; Aghapa, A. A.; Jafari, S. J.; Taghipour, S.; Bargeshadi, R., Photo degradation of Ceftriaxone in Aqueous Solution by Using UVC and UVC/H_2O_2 Oxidation Processes. *Appl. Water Sci.* **2019**, *9*, 81, DOI: 10.1007/s13201-019-0964-2.